N94-12302

Local isotropy in high Reynolds number turbulent shear flows

By Seyed G. Saddoughi

1. Motivation and background

This is a report on the continuation of the experiments, which Dr. Srinivas Veeravalli and the present author started in 1991, to investigate the hypothesis of local isotropy in shear flows. This hypothesis, which states that at sufficiently high Reynolds numbers the small-scale structures of turbulent motions are independent of large-scale structures and mean deformations (Kolmogorov 1941, 1962), has been used in theoretical studies of turbulence and computational methods like large-eddy simulation. The importance of Kolmogorov's ideas arises from the fact that they create a foundation for turbulence theory.

Local isotropy greatly simplifies the problem of turbulence. The total average turbulent energy dissipation ϵ, which in the usual tensor notation is given by

$$\epsilon = \nu \overline{\left(\frac{\partial u_i}{\partial x_j} + \frac{\partial u_j}{\partial x_i}\right)\frac{\partial u_j}{\partial x_i}}, \tag{1}$$

(summation on repeated indices) reduces to $\epsilon = 15\nu\overline{(\partial u/\partial x)^2}$, in locally isotropic turbulence (see Taylor 1935).

In the high-wavenumber region of the spectrum, Kolmogorov's universal equilibrium hypothesis implies that $E_{11}(k_1)/(\epsilon\nu^5)^{\frac{1}{4}}$ is a universal function of $(k_1\eta)$, where $\int_0^\infty E_{11}(k_1)\,dk_1 = \overline{u^2}$, k_1 is the longitudinal wavenumber and $\eta = (\nu^3/\epsilon)^{\frac{1}{4}}$ is the Kolmogorov length scale.

If the motion is isotropic, the transverse spectra $E_{22}(k_1)$ (for the velocity component normal to the wall) and $E_{33}(k_1)$ (for the spanwise component) are uniquely determined by the longitudinal spectrum (Batchelor 1953):

$$E_{22}(k_1) = E_{33}(k_1) = \frac{1}{2}(1 - k_1\frac{\partial}{\partial k_1})E_{11}(k_1). \tag{2}$$

In the inertial subrange, the 3D spectrum takes the form (Kolmogorov 1941)

$$E(k) = C\epsilon^{2/3}k^{-5/3}, \tag{3}$$

where k is the wavenumber magnitude, and, assuming isotropy, the one-dimensional longitudinal and transverse spectra are

$$E_{11}(k_1) = C_1\epsilon^{2/3}k_1^{-5/3} \tag{4}$$

and

$$E_{22}(k_1) = E_{33}(k_1) = C_1'\epsilon^{2/3}k_1^{-5/3} \tag{5}$$

respectively. The Kolmogoróv constant C is equal to $\frac{55}{18}C_1$, and equation (2) evaluated in the inertial subrange gives $C_1'/C_1 = 4/3$.

In isotropic flow the shear-stress co-spectrum, $E_{12}(k_1)$, defined by $\int_0^\infty E_{12}(k_1)\,dk_1 = -\overline{uv}$, is equal to zero. This indicates that for local isotropy to be satisfied, the normalized shear-stress co-spectrum,

$$R_{12}(k_1) = -E_{12}(k_1)[E_{11}(k_1)E_{22}(k_1)]^{-1/2}, \tag{6}$$

should roll-off at high wavenumbers.

Kolmogorov (1941) proposed scaling laws in the inertial subrange region for structure functions, which are moments of the velocity differences evaluated at points separated by longitudinal distances r. The second order longitudinal and transverse structure functions are given by

$$D_{11}(r) = \overline{[u(x+r) - u(x)]^2} = C_2\varepsilon^{2/3}r^{2/3} \tag{7}$$

and

$$D_{33}(r) = D_{22}(r) = \overline{[v(x+r) - v(x)]^2} = C_2'\varepsilon^{2/3}r^{2/3} \tag{8}$$

respectively, where $C_2 \approx 4C_1$ and $C_2'/C_2 = 4/3$. These are also known as Kolmogorov's 2/3 law. The third order longitudinal structure function was derived from the Navier-Stokes equations by Kolmogorov, without any appeal to self-similarity (Landau & Lifshitz 1987, p 140). In the inertial sub-range, this takes the following form;

$$D_{111}(r) = \overline{[u(x+r) - u(x)]^3} = -\frac{4}{5}\varepsilon r. \tag{9}$$

Our previous report (Veeravalli & Saddoughi 1991, hereinafter referred to as I), presented some spectral results taken at a single location in the boundary layer of the 80′ by 120′ wind tunnel at a freestream velocity of 40 m/s. These data indicated that the w-spectrum followed, but the v-spectrum deviated from (by a large amount) the isotropic relation in the inertial subrange region. No definite statement could be made for the dissipating eddies because our measurements were contaminated by high-frequency electrical noise. Some of the shortcomings of those measurements and their eventual improvement for the present experiments are discussed below in section 2.1.

In I, we also presented a short review of the work on local isotropy. Further, George & Hussein (1991) and Antonia, Kim & Browne (1991) have proposed that in shear flows the local-isotropy assumption should be relaxed to one of local axisymmetry (invariance with respect to rotation about the streamwise direction) and showed that the derivative moments obtained by experiments and by DNS in low-Reynolds-number flows supported the local-axisymmetry assumption. In I, it was concluded that, despite the many experiments conducted in a variety of flows to examine the validity of the local-isotropy hypothesis in shear flows, it appeared that there was no consensus regarding this concept in the scientific community. This conclusion still holds today. While the measurements in I were mainly intended as a *feasibility* study, it is hoped that the results presented here will enhance our understanding of the local-isotropy hypothesis.

2. Accomplishments

2.1. Apparatus and measurement techniques

The experiments described here were conducted at nominal freestream velocities (U_e) of 10 and 50 m/s in the boundary layer on the test-section ceiling of the full scale aerodynamics facility at NASA Ames. The test section is 80' high, 120' wide, and approximately 155' long. All four walls of the test section are lined with acoustic paneling, yielding a rough-wall boundary layer. The measurement station was located towards the end of the test section on the centerline of the tunnel. The data recording equipment and a small calibration wind tunnel were installed in an attic above the ceiling.

Here we will highlight the modifications to the equipment used in I and only give a very brief description of the instrumentation and techniques for the present measurements. The full details are given by Saddoughi & Veeravalli (1992, hereinafter referred to as II). One of the major alterations was done to the traversing mechanism. In I, the hot-wire probe holders were permanently fixed to the traversing rod, and it was necessary to calibrate the hot-wires using a different set of probe holders and cables than those connected to the traverse. The hot-wires were disconnected from the bridges after the calibration and reconnected to the anemometers via the traverse cables and probe holders for the actual measurements. This can result in a change in the hot-wire characteristics and a deviation from the calibration (Perry 1982). For the present experiments, this problem was avoided by redesigning some parts of the traverse such that the same cables and probe holders were used during both the calibration and actual measurements, without disconnecting the hot-wires.

For I, the measurements were conducted during the NASA Ames "swing-shift" period from mid-afternoon to midnight. We found that during that shift the temperature in the calibration tunnel was about $8°C$ higher than the temperature inside the 80' by 120' wind tunnel. In I the intake of the blower of the calibration tunnel was packed with ice to overcome this problem. To ensure a uniform distribution of mean temperature at the exit of the calibration tunnel, copper wool was placed in the pipe which connected the output of the blower to the intake of the calibration tunnel. This method reduced the temperature difference between the calibration and the actual measurements but it did not give us a good control over the amount of temperature reduction. Furthermore, the calibration temperature rose as the ice melted. The present measurements were performed during the "graveyard" shift from midnight to mid-morning during which the difference between the temperatures in the attic and inside the tunnel is smaller. To allow a fairly good temperature adjustment for the calibration, the intake of the blower of the calibration tunnel was connected to an air-conditioner via pipes having valves for controlling the intake of cold air. While for I the hot-wires were operated with an overheat ratio of 1.8, for the present measurements this was set at 2.0, which further reduced the possibility of drift due temperature changes.

For the present experiments, we acquired the latest instruments, which have lower background noise than those used for I. In addition, all of our electronic equipment was connected to an Oneac Power Conditioner (CB 1115) and Uninterruptible Power

System (UPS Clary PC 1.25K), which supplied clean power and prevented loss of data due to power failure. We also expanded our data acquisition capability from simultaneous sampling of two to sampling of six time-series.

At this stage, it is important to elaborate on another major difficulty encountered during I. Figure 1(a) shows the longitudinal spectrum obtained in I at $y/\delta \approx 1.4$ at a nominal freestream velocity of 40 m/s. Note, apart from the apparent spikes, the rise in the tail of the spectrum with frequency before the final roll-off due to the low-pass filtering (cut-off set at 100 kHz). This rise, which apparently has a slope of 2, was of great concern since it took place in the same region as that of the expected Kolmogorov frequency for that speed.

To ensure that this was not peculiar to the flow inside the 80' by 120' wind tunnel, spectra were taken, both in the attic of the 80' by 120' tunnel and at the Stanford laboratory, in the freestream of our calibration tunnel at the same velocity and filter cut-off frequency as those above. These spectra, Figure 1(b), clearly show the same problem being present in both the experimental facilities. Furthermore, to isolate the source of this problem, the spectra were measured in the freestream of the calibration tunnel at the Stanford laboratory using hot-wire bridges manufactured by different companies (TSI, Dantec, and one designed by Dr. Watmuff of the Fluid Mechanics Laboratory at NASA Ames). These results are shown in Figure 1(c). Again it appears that, as far as this phenomenon is concerned, the responses of all three bridges are similar. Finally, with a TSI IFA-100 bridge, spectra were taken in still air with 2.5 μm Tungsten wires and also with a standard fuse wire. These data are compared in Figure 1(d), where the same trend is clearly present.

The conclusion drawn from these tests is that when the turbulent energy of the flow is very small, the performance of the hot-wire bridges at high frequencies is limited by this phenomenon. This means that at the freestream velocity of 50 m/s, where the Kolmogorov frequency near the mid-layer of the boundary layer is of the order of 60 kHz, this rise in the tail of the spectrum is inevitable. In I it was suggested that, to allow accurate measurement of the dissipation range of the spectrum in this facility, experiments ought to be conducted at a nominal freestream velocity of 10 m/s, where the expected Kolmogorov frequency would be of the order of 5 kHz and this phenomenon could be avoided. As will be shown later, this aim has been accomplished.

Unlike the experiments in I, where data were obtained while NASA engineers were investigating the flow around an F-18 fighter aircraft in the central region of the working section, the present experiments were performed in an empty tunnel fully dedicated to our experiment.

The hot-wire instrumentation consisted of Dantec models 55P01 single wire and 55P51 cross-wire probes, modified to support 2.5 μm Platinum plated Tungsten wires with an etched length of approximately 0.5 mm, TSI IFA-100 model 150 hot-wire bridges, and model 157 signal conditioners. The high-pass and low-pass filters were Frequency Devices model 9016 (Butterworth, 48dB/octave). The hot-wire output voltages were digitized on a micro computer equipped with two Adtek AD830 12-bit analog-to-digital converters. To improve the frequency bandwidth of
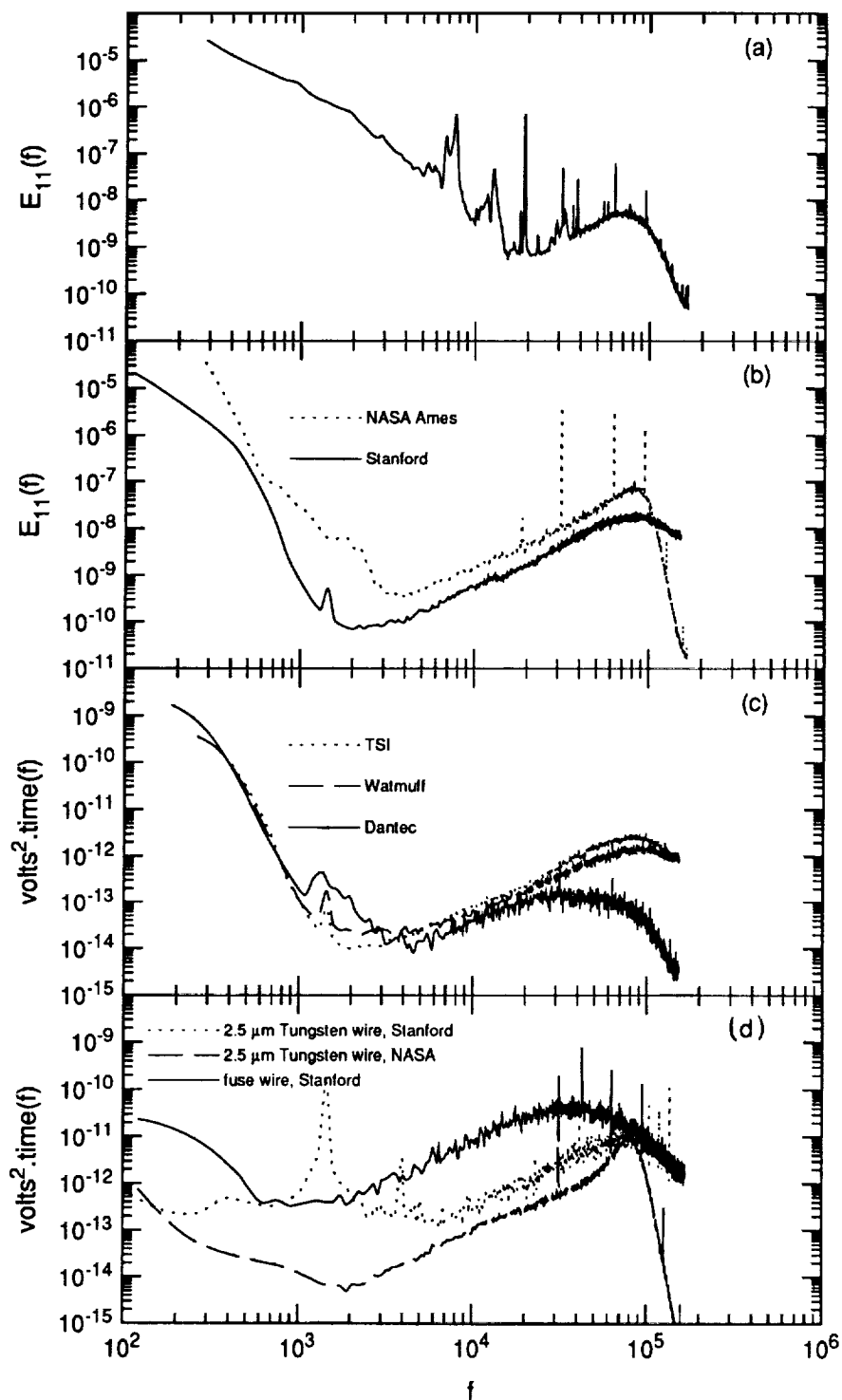
FIGURE 1. Comparison of noise spectra measured under different experimental conditions. (a) NASA 80- by 120-foot wind tunnel at freestream velocity of 40 m/s from I. (b) Calibration tunnel freestream at NASA and Stanford. (c) Calibration tunnel freestream at Stanford with different bridges. (d) TSI IFA-100 bridges with different wires in still air.

the spectrum at low frequencies, the data were obtained in three spectral bands. For the low-speed measurements around the mid-layer, these three bands were 0.1 Hz to 100 Hz, 0.1 Hz to 1 kHz, and 0.1 Hz to 10 kHz, which were chosen to resolve the large scales, inertial range, and the dissipation region respectively. The corresponding bands for the high-speed case were 0.1 Hz to 1 kHz, 0.1 Hz to 20 kHz, and 0.1 Hz to 100 kHz. In I, for each spectral segment, the high-pass filter-cutoff frequency was increased. The advantage of this method was that it permitted us to change the dynamic range of the analog-to-digital convertor to match that expected in a given band. However, recall from Figure 1 that a good resolution of the high-frequency end of the spectrum at high-speeds was not necessary since that part of the spectrum was contaminated by the f^2 behavior. It will be shown in section 2.2 that as expected, keeping all the other parameters the same, this change in the high-pass cutoff frequency did not affect our results.

In general, for spectral measurements, 200 records of 4096 samples each were recorded in the low-frequency band and 400 such records in the higher-frequency bands. In each case, the sampling frequency was three to four times larger than the low-pass filter cut-off frequency in order to avoid aliasing errors. The spectral density of each band was computed by a fast-Fourier-transform algorithm. To convert frequencies to wavenumbers, Taylor's hypothesis was used. The time series for both the X-wires (UV- and UW-mode) and the single wire were obtained simultaneously. For the low-speed experiment the measurement positions were at $y/\delta \approx 0.025$, 0.1, 0.3, 0.5, 0.9 and for the high-speed case they were at $y/\delta \approx 0.1$, 0.4, 0.8. Here we only present the data taken around mid-layer at both freestream velocities. These, as well as the results taken at other y/δ positions, are given in II.

2.2. Results and discussion

It is shown in II that the large-scale characteristics of the boundary layer followed the standard behavior in the outer part of the layer at both nominal freestream velocities of 10 m/s and 50 m/s. Also, it appeared that the thickness of the boundary layer, δ, in both cases was about the same ($\approx 1m$) at this measurement location. It is important to emphasize that the objective of the present experiments is not to investigate the concept of local isotropy in a canonical boundary layer. However, if it so happens that the boundary layer behaved reasonably close to the canonical form, this would be considered a bonus.

The mid-layer position is perhaps the best point at which to analyze the spectral results because of its following advantages: (a) the rms longitudinal velocity fluctuation normalized by the local mean velocity, $\sqrt{\overline{u^2}}/U$, is less than 0.1, so that errors arising from the use of Taylor's hypothesis will be small (Lumley 1965); (b) the Reynolds number R_λ ($\equiv \sqrt{\overline{u^2}}\lambda/\nu$), based on the Taylor microscale λ [$\equiv \sqrt{\overline{u^2}/(\partial u/\partial x)^2}$] is close to its maximum value, and (c) it is well inside the layer so that boundary-layer edge intermittency effects are not present.

The main aim of the present study has been to investigate the effects of mean-strain rate ($S = \partial U/\partial y$) on local isotropy. The non-dimensional quantity

$$S^* = \frac{Sq^2}{\varepsilon},\tag{10}$$

the shear-rate parameter, which is the ratio of the eddy turnover time (q^2/ε) to the timescale of mean deformation (S^{-1}), characterizes the effects of mean-strain rate on the turbulence (Moin 1990; Lee, Kim & Moin 1990). Durbin & Speziale (1991) examined the equation for the dissipation rate tensor and showed that local isotropy is inconsistent with the presence of mean-strain rate. The profile of shear-rate parameter for a turbulent channel flow (Lee, Kim & Moin 1990), reached its maximum value of about 35 at y^+ ($= yU_\tau/\nu$, where U_τ is the friction velocity) ≈ 10 in the viscous sublayer and decreased to a value of about 6 for $y^+ > 50$.

On the other hand, Corrsin (1958) proposed that local isotropy in shear flows can exist when

$$S_c^* = \frac{(\frac{\nu}{\varepsilon})^{1/2}}{S^{-1}} \ll 1.\tag{11}$$

This is the ratio of the Kolmogorov and mean-shear timescales. The channel-flow profile of S_c^*, presented by Antonia & Kim (1992), indicates a constant value of about 2.5 in the viscous sublayer and a reduction to a very small values for $y^+ > 60$. These authors suggested that the Corrsin criterion is too restrictive and may be relaxed to $S_c^* \leq 0.2$ for the small scales to be isotropic.

Table 1. shows the flow parameters for spectral measurements at mid-layer location. In general, there is some degree of uncertainty associated with the estimation of S^* and S_c^* because they involve gradients at data points that are widely spaced, and, as will be shown later, the dissipation values are accurate to 20%. In Table 1, it can be seen that the value of $S^*/\sqrt{R_\lambda}$ becomes independent of freestream velocity. It is shown in II that as the wall is approached the values of these two parameters increase, and, at a given y/δ, the trend seen in Table 1 prevails.

Freestream velocity, U_e (m/s)	≈ 50	≈ 10
Boundary layer thickness, δ (m)	≈ 1.0	≈ 1.0
Measurement location, y/δ	≈ 0.4	≈ 0.5
Local mean velocity, U (m/s)	$= 43.2$	$= 8.95$
Local turbulence intensity, $\sqrt{\overline{u^2}}/U$	$= 0.07$	$= 0.065$
Microscale Reynolds number, R_λ	≈ 1500	≈ 600
Ratio of hot-wire length, l to η	≈ 5	≈ 1.5
Shear-rate parameter, S^*	≈ 8	≈ 5
$S^*/\sqrt{R_\lambda}$	≈ 0.21	≈ 0.21
Corrsin parameter, S_c^*	≈ 0.0107	≈ 0.016

TABLE 1: Flow parameters for spectral measurements around mid-layer.
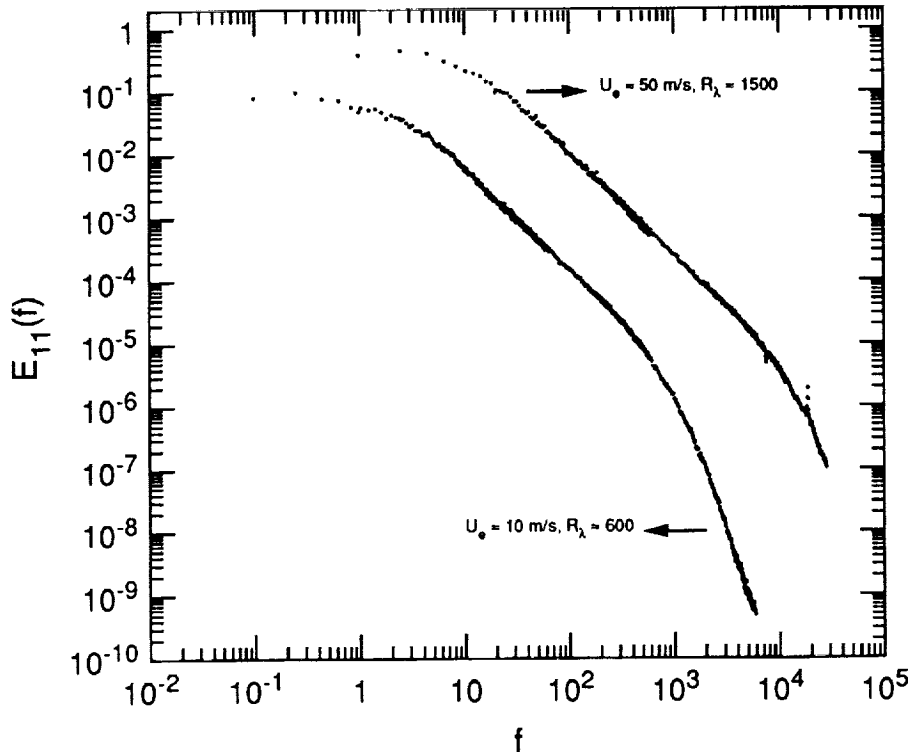
FIGURE 2.   Longitudinal power spectra measured around mid-layer at different freestream velocities.

Figure 2 shows $E_{11}(f)$ for both freestream velocities, obtained in the three measurement bands given in section 2.1. Clearly, in each case, the agreement between the three segments of the spectrum is very good. The collapse for the transverse spectra was equally good. The Kolmogorov frequencies, $f_\eta (= U/2\pi\eta$, where η was calculated by using the isotropic relation) were about 69 kHz and 4.5 kHz for the high- and low-speed measurements respectively. To avoid the f^2 behavior of the tail of the spectrum (section 2.1), and also due to lack of sufficient spatial resolution (Wyngaard 1968; Ewing & George 1992), only frequencies up to about 30 kHz could be resolved for the high-speed case. However, for the low-speed measurements, five-decades of frequency were obtained with no contamination from electronics noise and with good spatial resolution. As explained in section 2.1, the low-speed measurements were required mainly to resolve the dissipation range of the spectrum, but it is important to bear in mind that the high-speed results are more appropriate for the investigation of inertial-subrange scaling because they are at a much higher R_λ. It will become clear in the following sections that without the measurements at 50 m/s in the inertial range, one may reach erroneous conclusions.

Figure 3, which is plotted with Kolmogorov scaling, shows a comparison between the present data and a compilation of some experimental work taken from Chapman (1979) with later additions. The agreement is good. With this type of scaling, the
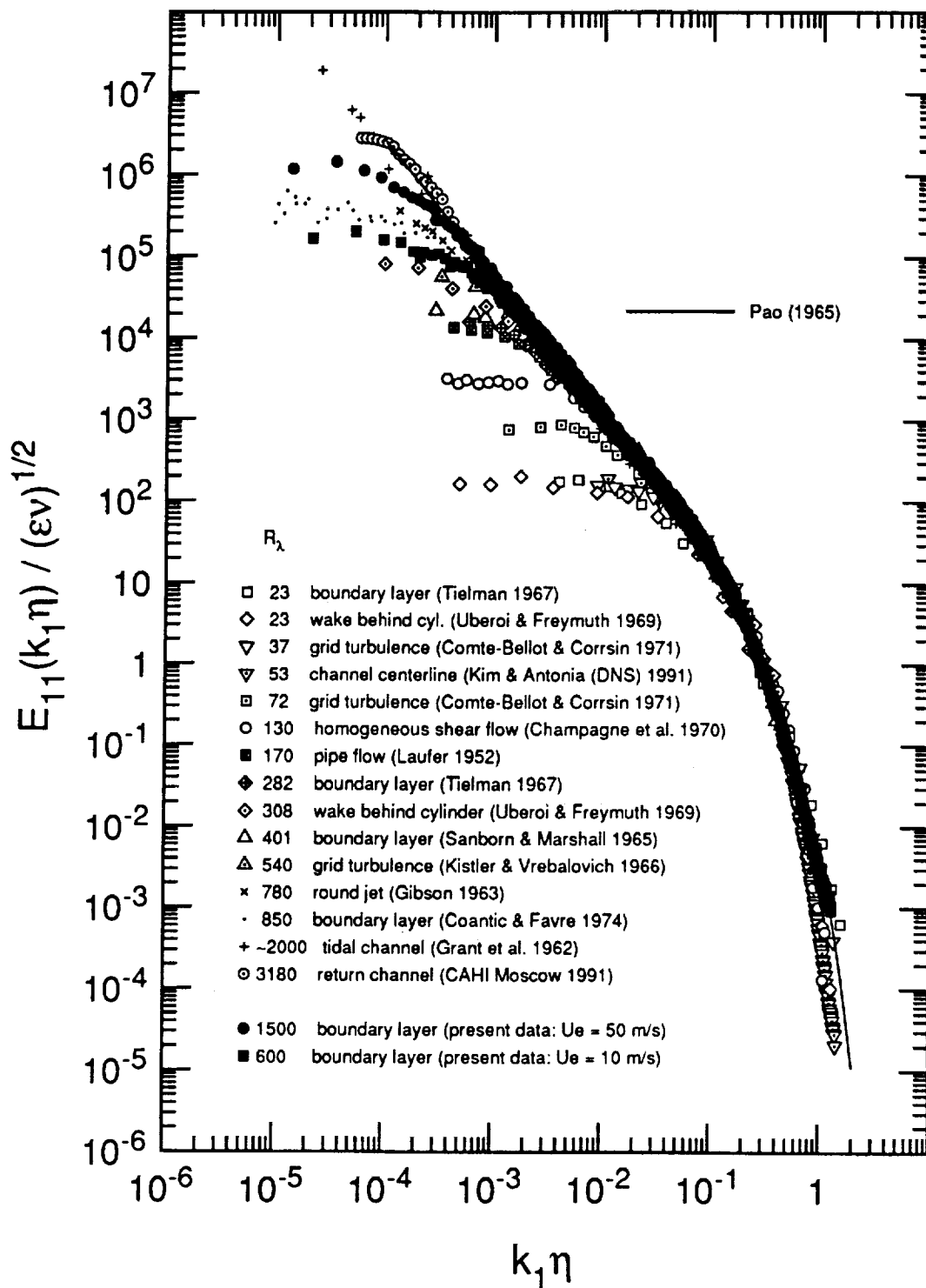
$E_{11}(k_1\eta)/(\varepsilon\nu)^{1/2}$

10^7
10^6
10^5
10^4
10^3
10^2
10
1
10^{-1}
10^{-2}
10^{-3}
10^{-4}
10^{-5}
10^{-6}

10^{-6} 10^{-5} 10^{-4} 10^{-3} 10^{-2} 10^{-1} 1

$k_1\eta$

Pao (1965)

R_λ

□	23	boundary layer (Tielman 1967)
◇	23	wake behind cyl. (Uberoi & Freymuth 1969)
▽	37	grid turbulence (Comte-Bellot & Corrsin 1971)
▽	53	channel centerline (Kim & Antonia (DNS) 1991)
⊡	72	grid turbulence (Comte-Bellot & Corrsin 1971)
O	130	homogeneous shear flow (Champagne et al. 1970)
■	170	pipe flow (Laufer 1952)
◆	282	boundary layer (Tielman 1967)
◇	308	wake behind cylinder (Uberoi & Freymuth 1969)
△	401	boundary layer (Sanborn & Marshall 1965)
△	540	grid turbulence (Kistler & Vrebalovich 1966)
×	780	round jet (Gibson 1963)
·	850	boundary layer (Coantic & Favre 1974)
+	~2000	tidal channel (Grant et al. 1962)
⊙	3180	return channel (CAHI Moscow 1991)
●	1500	boundary layer (present data: Ue = 50 m/s)
■	600	boundary layer (present data: Ue = 10 m/s)

FIGURE 3. Kolmogorov scaling for the longitudinal spectra compared with data from other experiments. This compilation is from Chapman (1979) with later additions.
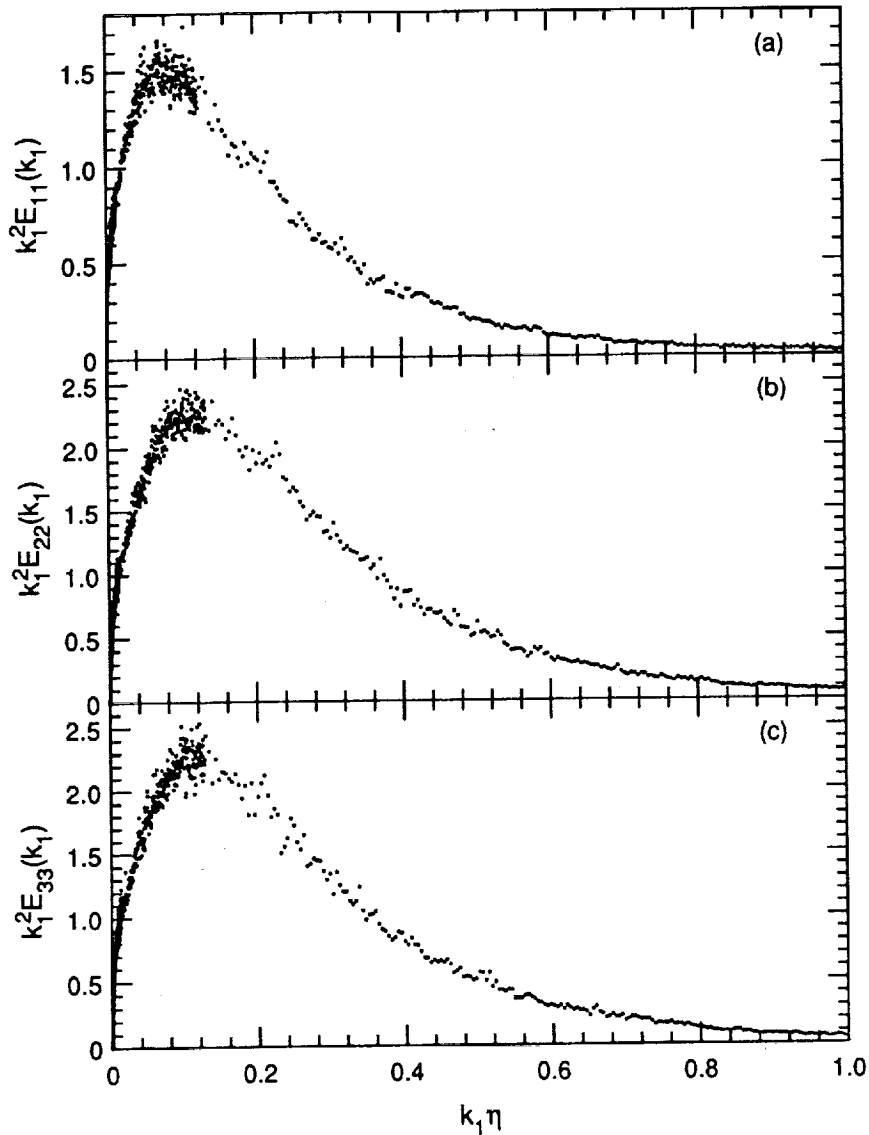
FIGURE 4.   Dissipation spectra measured at $y/\delta \approx 0.5$ for $U_e \approx 10 \ m/s$ and $R_\lambda \approx 600$. (a) u-spectrum; (b) v-spectrum; (c) w-spectrum.

spectra peel off from the $-5/3$ law at the low-wavenumber end in order of increasing Reynolds number. The present spectrum for $R_\lambda \approx 1500$ has a $-5/3$ slope over approximately two decades in wavenumber; one of the longest $-5/3$ ranges seen in laboratory flows.

For $U_e \approx 10 \ m/s$ and $R_\lambda \approx 600$, dissipation spectra defined by the isotropic relation, $\varepsilon = 15\nu \int_0^\infty k_1^2 E_{11}(k_1)dk_1 = 7.5\nu \int_0^\infty k_1^2 E_{22}(k_1)dk_1 = 7.5\nu \int_0^\infty k_1^2 E_{33}(k_1)dk_1$, are plotted in Figure 4. For $R_\lambda \approx 1500$, a similar plot for only the u-spectrum is shown in Figure 5. These figures show that in the high-speed case, it is only possible to take measurements up to $k_1\eta \approx 0.4$, but for the low-speed experiments,
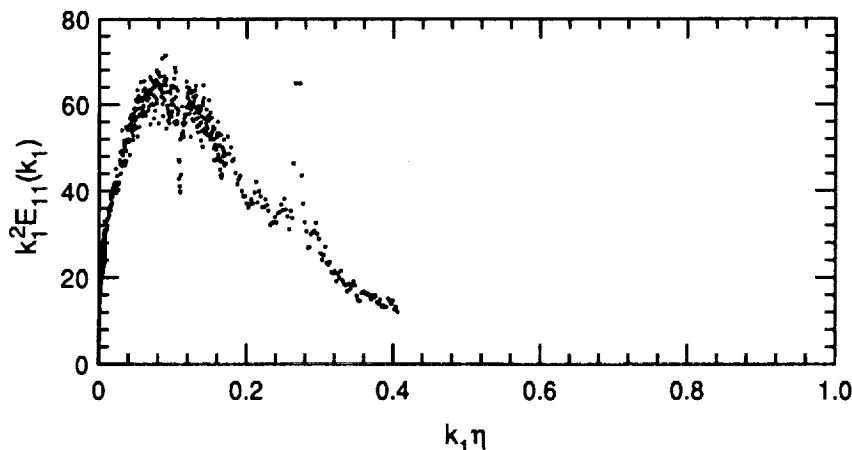
FIGURE 5. Dissipation spectrum measured at $y/\delta \approx 0.4$ for $U_e \approx 50$ m/s and $R_\lambda \approx 1500$.

the entire dissipation spectrum is obtained. However, for $R_\lambda \approx 600$ the scatter of the data around the peak is about $\pm 10\%$, and, as will be shown later, the data for $k_1\eta > 0.9$ may not be reliable. The integrations of these data satisfy the above isotropic relation to within 10%.

To investigate the isotropy of scales within the inertial subrange, we use equations (4) and (5) and analyze the compensated spectra $k_1^{5/3}E_{ii}(k_1)$, where $i = 1, 2$ or 3 (no summation over i) corresponds to u, v, or w respectively. In the inertial subrange, these compensated spectra should be independent of wavenumber, and the v- and w-spectra should be equal to each other and larger than the u-spectrum by a factor $4/3$.

In Figure 6, the compensated spectra for $U_e \approx 10$ m/s, $R_\lambda \approx 600$ are plotted against $k_1\eta$. The 9th-order, least-square polynomial fit to these data presented in Figure 7 prove to be very instructive in analyzing the data. Using the dissipation value ($\epsilon \approx 0.33$ m^2/s^3) obtained by integrating over the third-spectral band, which covered the entire frequency range of interest in Figure 4(a), and taking the classical value for the Kolmogorov constant, $C = 1.5$ (i.e. $C_1 \approx 0.5$), the isotropic values in the inertial subrange for the compensated spectra were calculated. These are shown as straight lines in Figures 6 and 7. For the u-spectrum, shown in Figure 7, there is slightly less than one decade of $-5/3$ region, and in that region $C = 1.5$ agrees well with the present data. Noting that our dissipation accuracy was to $\pm 10\%$, this gives $C = 1.5 \pm 0.1$. The w-spectrum shows more than half a decade of $-5/3$ region, with an amplitude equal to $4/3$ times that of the u-spectrum (the difference between the flat region of the w-spectrum and the isotropic line is about 5%). However, it appears that in the region under consideration, the v-spectrum does not show a perfectly flat portion. It will be shown later that this is a Reynolds number effect. All three spectra have a "bump" between the inertial subrange and the dissipation range. These "bumps" have also been observed in other experiments (Williams & Paulson 1978 and Champagne, Friehe, LaRue & Wyngaard 1977 for temperature variance spectra; Mestayer 1982 for velocity spectra) and theoretical predictions
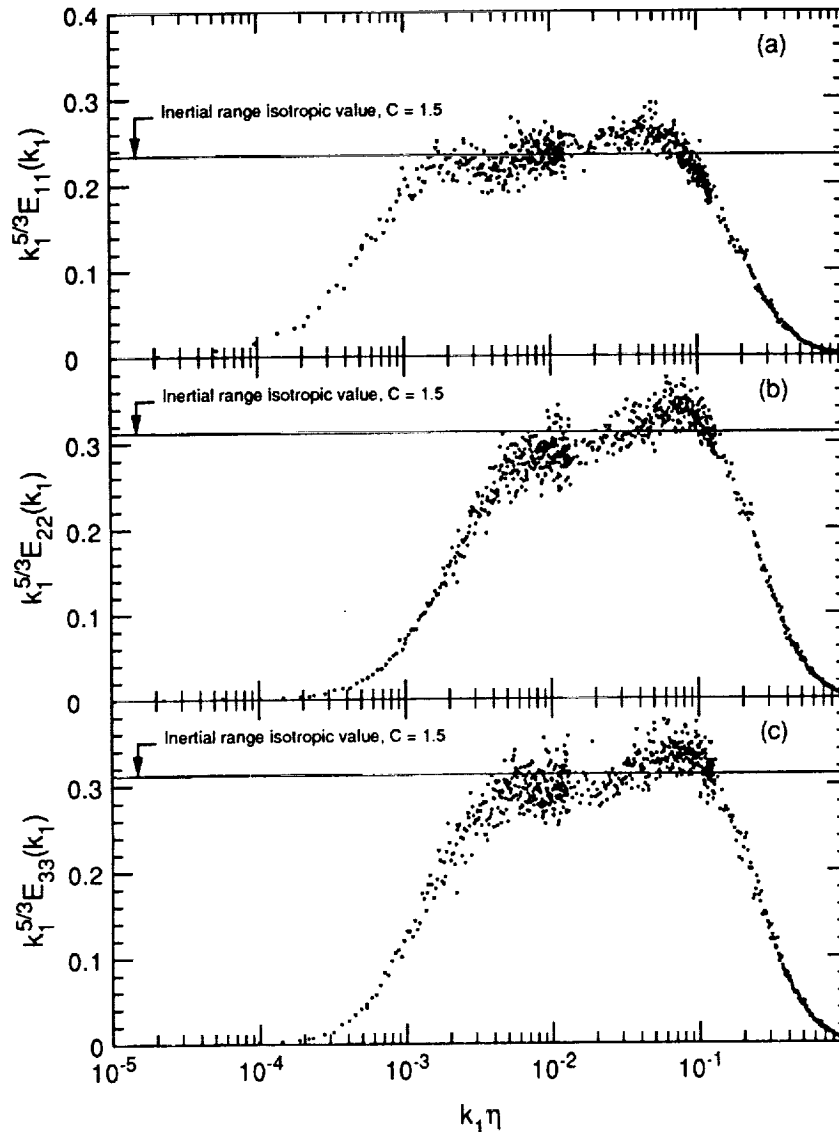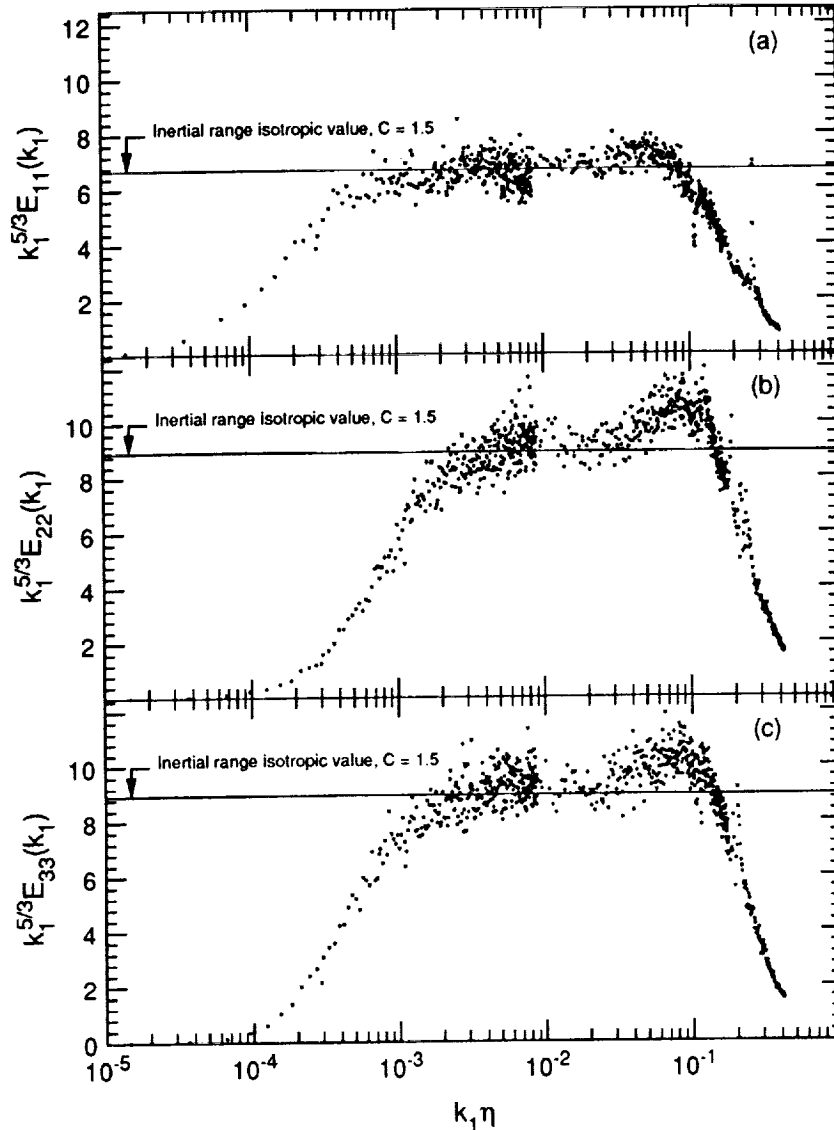
S. G. Saddoughi

FIGURE 6. Compensated longitudinal and transverse spectra measured around mid-layer for $U_e \approx 10$ m/s and $R_\lambda \approx 600$. (a) u-spectrum; (b) v-spectrum; (c) w-spectrum.

such as Eddy-Damped Quasi-Normal Markovian (EDQNM), as discussed by Mestayer, Chollet & Lesieur (1984). Also, in his review talk, Saffman (1992) mentioned the existence of this "bump" in the 3D-spectrum.

The compensated spectra and their corresponding 9th-order polynomial fits for $U_e \approx 50$ m/s, $R_\lambda \approx 1500$, are shown in Figures 8 and 9 respectively. It is clear that for these high-speed data, a good estimate for dissipation is not possible (see Figure 5). However, since our low-speed data indicates that $C = 1.5 \pm 0.1$, we will use this value and the fitted isotropic lines shown in Figures 8 and 9, to calculate $\epsilon \approx 49$
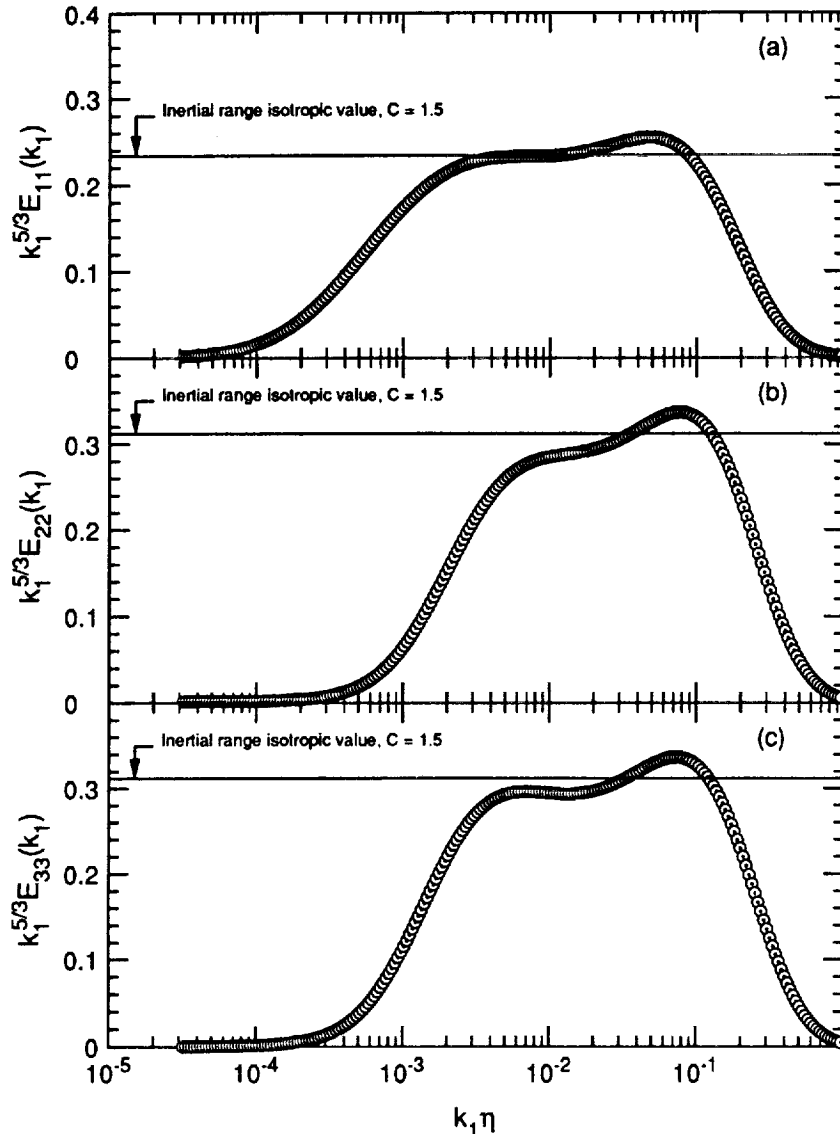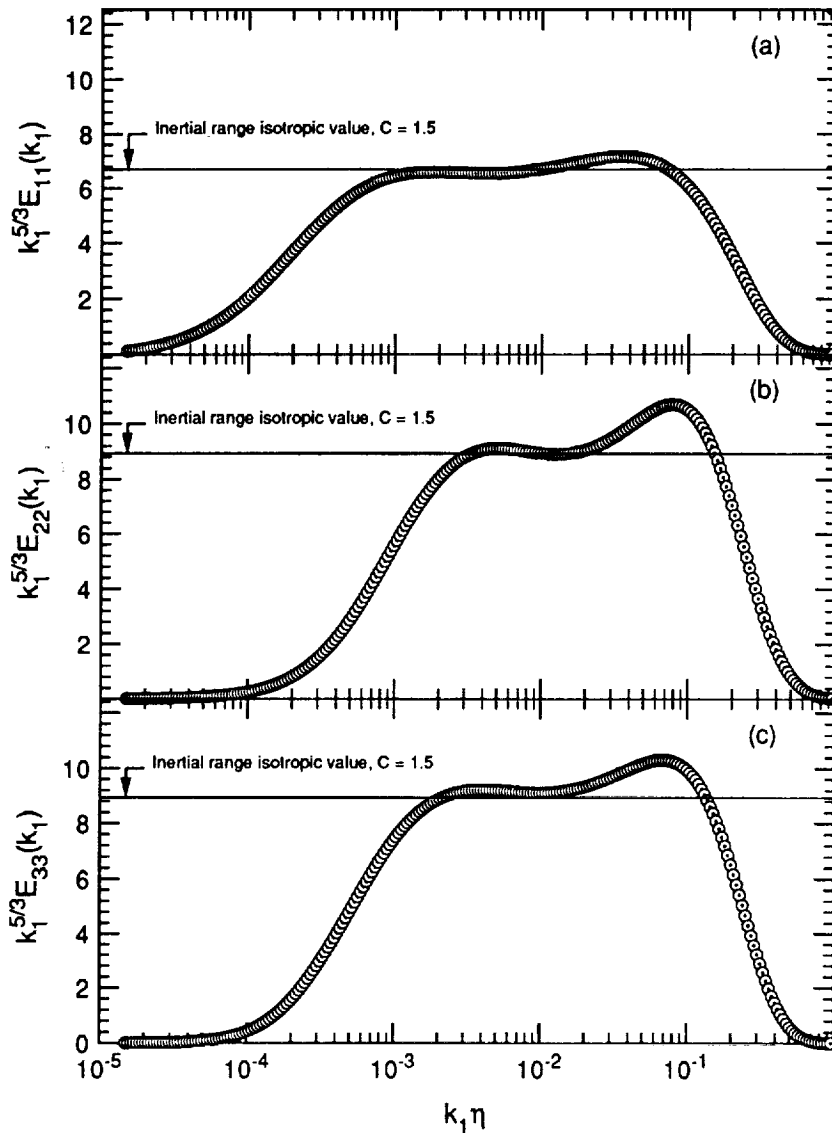
FIGURE 7. Compensated spectra obtained from 9th-order, least-square polynomial fits to the data presented in Figure 6.

m^2/s^3. We will show later in the discussion of the third-order structure functions that this estimation is within the 20% uncertainty associated with our dissipation calculations. It can be seen from Figure 9 that for the higher R_λ, the compensated u-spectrum exhibits more than one decade of $-5/3$ region, but less than the log-log plot (Figure 3) suggested. Here the v-spectrum, as well as the w-spectrum contain well defined $-5/3$ inertial-subrange regions. They are, as predicted, equal to each other and are larger than the u-spectrum by the $4/3$ factor. The "bumps" again appear on all the three spectra at almost the same $k_1\eta$ as for the low-speed case. There is no indication that the amplitude of the "bump" reduces with increasing

FIGURE 8.   Compensated longitudinal and transverse spectra measured around mid-layer for $U_e \approx 50\ m/s$ and $R_\lambda \approx 1500$. (a) u-spectrum; (b) v-spectrum; (c) w-spectrum.

Reynolds number once a well-defined inertial subrange is present.

The above observations suggest that only the linear-log plot of compensated spectra can clearly show these intricate behaviors in the inertial-subrange region. Any claim for the existence of an inertial subrange should be substantiated with this kind of plot. Recall from Table 1 that the high-speed S^* value was larger than that of the low-speed case, which apparently indicates that here the deviation from the isotropic relations of the v-spectrum is mainly a function of the Reynolds number. Mestayer (1982), who presented u- and v-spectra (no w-spectrum was measured)

FIGURE 9. Compensated spectra obtained from 9th-order, least-square polynomial fits to the data presented in Figure 8.

for only one position ($y/\delta = 0.33$) in a boundary layer at $R_\lambda \approx 616$ and $S_c^* = 0.02$, concluded that the local-isotropy criterion was not satisfied in the inertial-subrange region. Our measurements indicate that in his flow the Reynolds number was not large enough to produce $-5/3$ regions in the spectra.

The ratio of the measured w-spectrum to v-spectrum, $E_{33}^{meas}(k_1)/E_{22}^{meas}(k_1)$, in the inertial and the dissipation ranges should be equal to 1.0 if the turbulence is isotropic. As mentioned earlier, in I, for measurements at $y/\delta \approx 0.4$, $U_e \approx 40$ m/s and $R_\lambda \approx 1450$, this ratio deviated substantially from unity. Figure 10 shows the ratio of these spectra from I. The present measurements of this ratio at $y/\delta \approx 0.4$
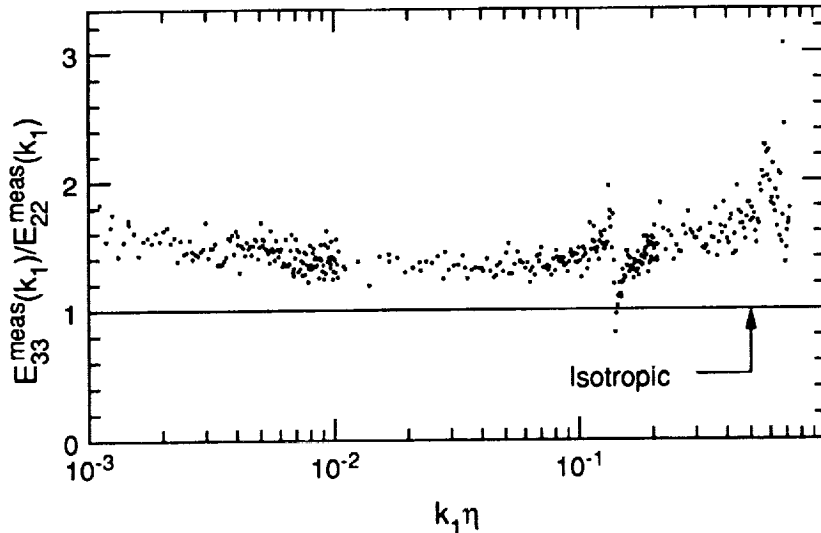
FIGURE 10. Ratio of the measured w-spectrum to v-spectrum at $y/\delta \approx 0.4$ for $U_e \approx 40 \ m/s$ and $R_\lambda \approx 1450$ obtained in I.

for $R_\lambda \approx 1500$ are shown in Figure 11. The three plots of Figure 11 present data taken with different sets of X-wires having different calibrations. The data in Figure 11(c) were measured with the same high-pass filter-cutoff frequencies as in I (see section 2.1). As can be seen, the day-to-day variation among the present data is $\pm 10\%$, a fairly good repeatability. The present data are quite different from I, and, in view of all the measurement problems encountered during I (see section 2.1), we have greater confidence in the present data.

The ratio of the spectra measured around mid-layer in the present experiments for both the freestream velocities are shown in Figure 12. For $R_\lambda \approx 600$ and $R_\lambda \approx 1500$, the w-spectrum becomes equal to v-spectrum, to $\pm 10\%$, for $k_1\eta > 2 \times 10^{-2}$ and $k_1\eta > 3 \times 10^{-3}$ respectively.

The transverse spectra, $E_{22}^{calc}(k_1)$ and $E_{33}^{calc}(k_1)$ can be calculated from the measured longitudinal spectrum, $E_{11}^{meas}(k_1)$ using equation (2). An anisotropy measure may be defined as $E_{ii}^{calc}(k_1)/E_{ii}^{meas}(k_1)$, where $i = 2$ or 3 corresponds to v or w respectively. These anisotropy measures should be equal to 1.0 in an isotropic flow. We have used least-square fit data that were shown in Figures 7 and 9 to calculate these measures, which are shown in Figure 13. It appears that in both cases the isotropic value (to $\pm 10\%$) is obtained for the dissipation regions, and for $R_\lambda \approx 1500$, local isotropy is indicated for the entire inertial subrange of the transverse spectra. For $R_\lambda \approx 600$, the anisotropy coefficients for v and w become equal to $1.0 \pm 10\%$ at about $k_1\eta > 8 \times 10^{-3}$ and $k_1\eta > 4 \times 10^{-3}$ respectively. Comparison of the low- and high-Reynolds-number cases suggests that for the latter case, the rise in the anisotropy coefficients at the high-wavenumber end is not real, but rather an artifact of extending the polynomial fit to a region where no data was available.
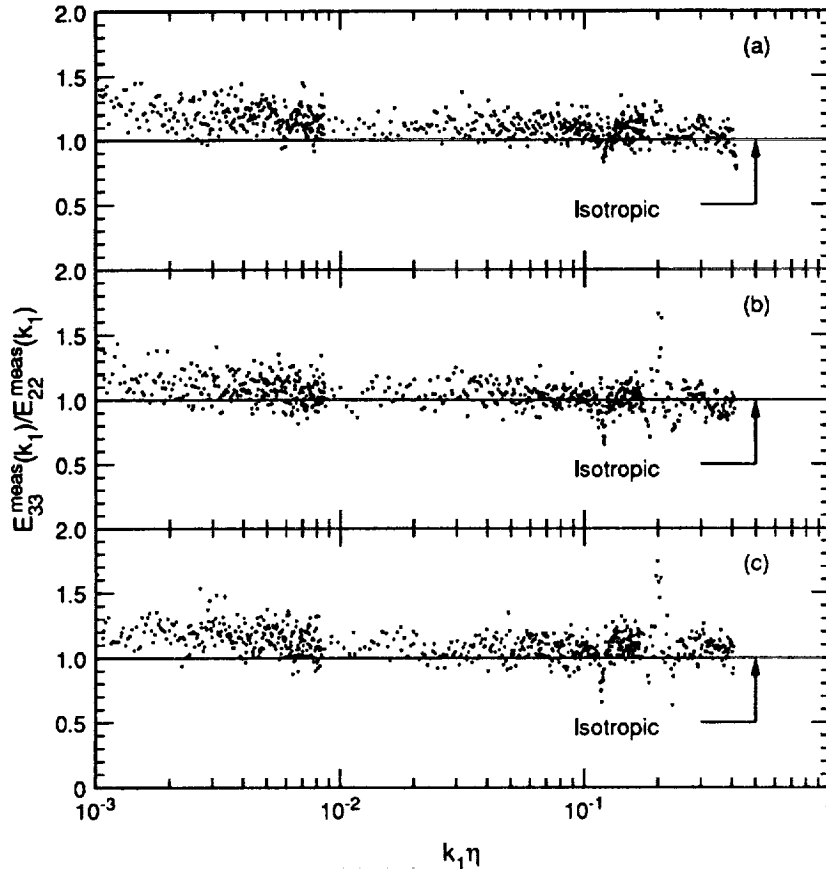
FIGURE 11.   Ratios of the measured w-spectrum to v-spectrum at $y/\delta \approx 0.4$ for $U_e \approx 50\ m/s$ and $R_\lambda \approx 1500$ obtained under different experimental conditions.

For both Reynolds numbers under consideration, the normalized shear-stress co-spectrum, defined by equation (6), are shown in Figure 14. As expected (e.g. Mestayer 1982; Nelkin & Nakano 1983), these spectra roll-off to zero at high wavenumbers after showing initial values of about 0.6 to 0.7 in the low-wavenumber region. However, for $R_\lambda \approx 1500$, this coefficient reaches the zero value about half a decade later than the start of the $-5/3$ region.

Kraichnan (1959) proposed that the dissipation region of the 3D energy spectrum has a simple exponential decay with an algebraic prefactor of the form,

$$E(k) = A(k\eta)^\alpha exp[-\beta(k\eta)].\qquad(12)$$

Since then, his form has also been found in numerical simulations (DNS), but necessarily at very low Reynolds numbers, by other researchers who have proposed that for $0.5 \leq k\eta \leq 3$, $\beta \approx 5.2$ (Kida & Murakami 1987; Kerr 1990; Sanda 1992; Kida *et al.* 1992). It can be readily seen that for a locally-isotropic turbulence, the form of equation (12) and the numerical value of β, what ever it may be, should
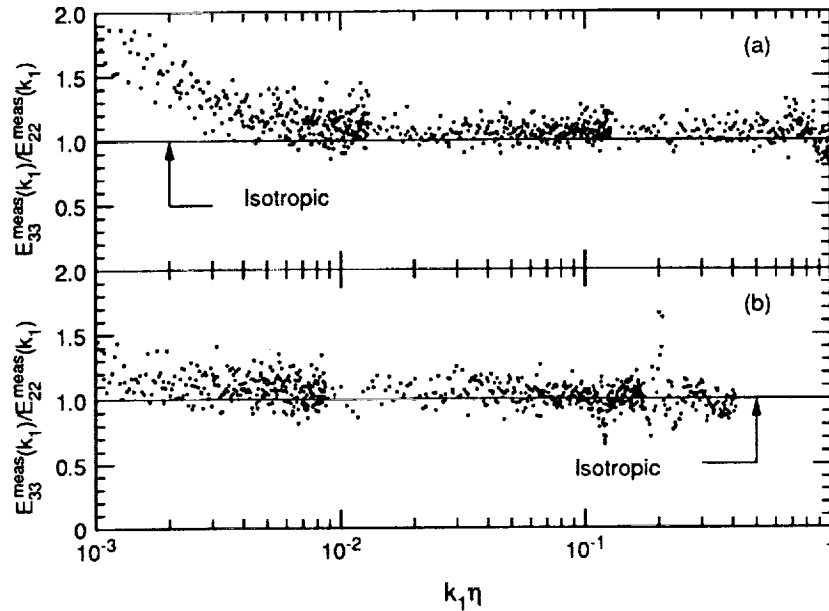
FIGURE 12.   Ratios of the measured w-spectrum to v-spectrum obtained around mid-layer. (a) $U_e \approx 10\ m/s$, $R_\lambda \approx 600$; (b) $U_e \approx 50\ m/s$, $R_\lambda \approx 1500$.

be preserved for all three one-dimensional spectra. The exponential form for the u-spectrum in the far-dissipation region was observed in experiments by Sreenivasan (1985), but he proposed $\beta = 8.8$ for $0.5 \leq k_1 \eta \leq 1.5$.

The compensated spectra can also be presented (see e.g. Smith & Reynolds 1991) as $\epsilon^{-2/3} k_1^{5/3} E_{ii}(k_1)$, where $i = 1$, 2 or 3 (no summation over i) corresponds to u, v or w respectively. Log-linear plots of these spectra at mid-layer for $R_\lambda \approx 600$ are shown in Figure 15. This figure also contains the low-speed spectra measured close to the wall at $y/\delta \approx 0.025$. It appears that in the dissipation region, all three components of spectra show an essentially exponential decay and follow reasonably well the straight lines with $\beta = 5.2$ for $0.5 \leq k_1 \eta \leq 1$. Note that for the u-spectrum, the flat region for $k_1 \eta \geq 0.9$ is perhaps due to noise and/or lack of resolution.

Local isotropy in the inertial subrange was also investigated, for consistency, with Kolmogorov's scaling laws for the structure functions, given by equations (7), (8), and (9). For both freestream velocities, the compensated third-order structure functions for the longitudinal velocity fluctuations, $(-5/4)r^{-1}D_{111}(r)$, are plotted versus (r/η) in Figure 16. With this scaling, the compensated third-order structure functions should become independent of r in the inertial subrange at a value equal to the dissipation. This is a good way to estimate ε if an inertial subrange exists. In each section of this figure, as explained in section 2.1, there are three different data sets corresponding to the three measurement bands used for resolving the large scales, inertial subrange, and the dissipation region. For $R_\lambda \approx 600$ and $R_\lambda \approx 1500$, about one-and-a-half and two decades of relatively flat regions can be seen respectively. The corresponding dissipation values taken from these plots were
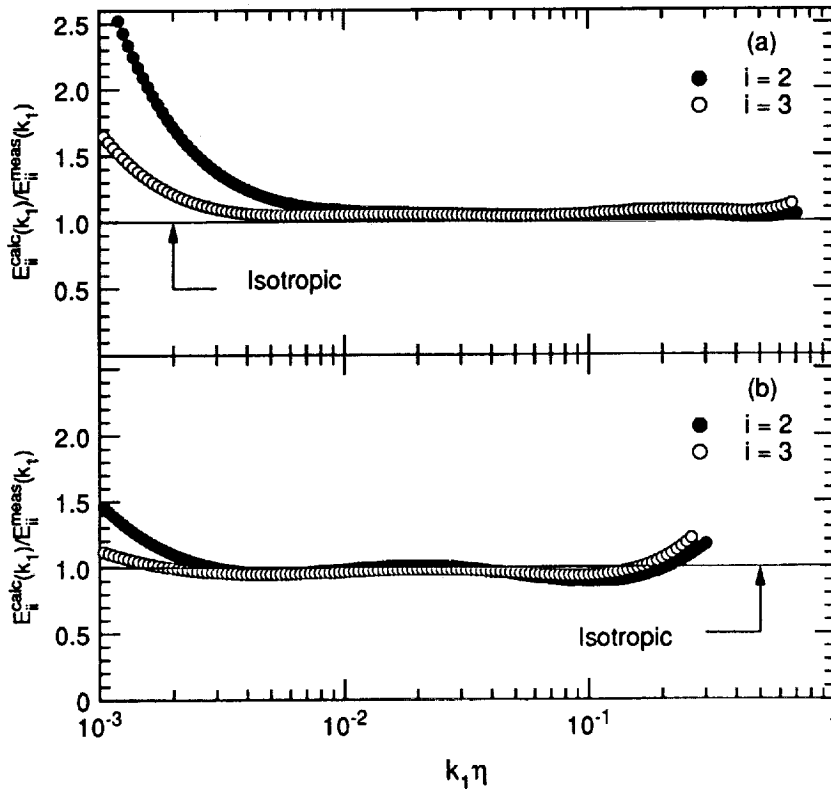
FIGURE 13. Anisotropy coefficients obtained around mid-layer. (a) $U_c \approx 10$ m/s, $R_\lambda \approx 600$; (b) $U_c \approx 50$ m/s, $R_\lambda \approx 1500$.

$\epsilon \approx 0.26$ m^2/s^3 and ≈ 40 m^2/s^3, which are about 20% lower than those estimated from the spectra.

For $R_\lambda \approx 600$, the second-order compensated structure functions, $r^{-2/3}D_{ii}(r)$, where $i = 1$, 2, or 3 correspond to u, v, or w respectively, are plotted in Figure 17. For $R_\lambda \approx 1500$, a similar plot is shown in II. The three components of the second-order structure functions showed inertial-subrange regions, albeit the v-component for the low-speed case shows the least extent. For each Reynolds number considered independently, the v- and w-structure functions in the inertial subrange are equal to each other and are larger than the u-structure function by the factor 4/3, to within the measurement accuracy. Taking the Kolmogorov constant $C_2 \approx 2$ and for each Reynolds number using the dissipation obtained from its respective third-order structure function, the isotropic values of the second-order structure functions can be calculated. For the low speed case, these are shown as straight lines in Figure 17. For the high-Reynolds-number case, the deviation of the straight lines from the plateau regions was equivalent to a 10% change in the dissipation; better agreement was obtained if the ϵ estimated from spectra was used (see II). Therefore, here $C_2 = 2.0 \pm 0.1$.

Overall, as the above tests show, it is important that the concept of local isotropy be investigated by different means. The linear-log plot of compensated spectra
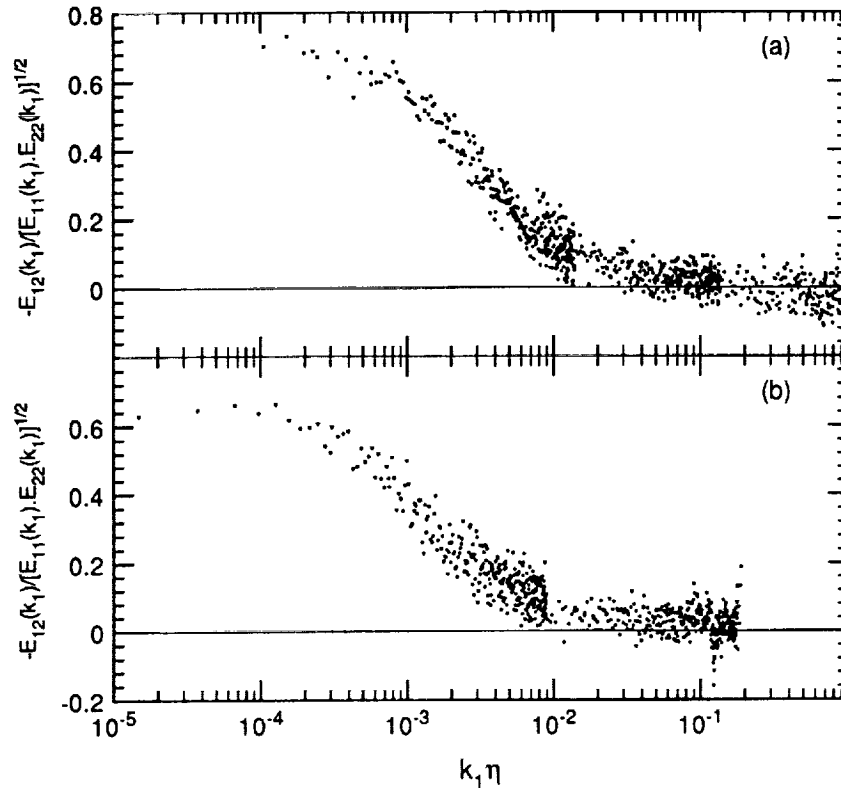
FIGURE 14. Normalized shear-stress co-spectra obtained around mid-layer. (a) $U_e \approx 10 \ m/s$, $R_\lambda \approx 600$; (b) $U_e \approx 50 \ m/s$, $R_\lambda \approx 1500$.

proved to be a very important test in the inertial-subrange region. The different sets of data taken around the mid-layer of the boundary layer at the two Reynolds numbers, $R_\lambda \approx 600$ and ≈ 1500, were complementary to each other. It appeared that the determining factor for the existence of a well-defined $-5/3$ region on all the three components of spectra was the Reynolds number: the v-spectrum appeared to be the most sensitive indicator of low R_λ effects. Spectral "bumps" between the inertial subrange and the dissipative region were observed on all the spectra. One may obtain an anomalously large Kolmogorov constant if these "bumps" are not identified. For the present experiments, we obtain $C = 1.5 \pm 0.1$ from the spectra and $C_2 = 2 \pm 0.1$ from the second-order structure functions. While in both high- and low-speed cases local isotropy is found (to $\pm 10\%$) in the dissipation regions, for $R_\lambda \approx 1500$, it was also found over the entire inertial subrange of the transverse spectra. However, the normalized shear-stress co-spectra reached the zero value about half of a decade later than the start of the $-5/3$ region. It was observed that in the dissipation region, all three components of spectra had an exponential decay and $\beta = 5.2$ for $0.5 \leq k_1\eta \leq 1$ agreed reasonably well with the present data.

In II we have analyzed the results taken in the log-layer at both nominal freestream velocities of $\approx 10 \ m/s$ and $\approx 50 \ m/s$. When the wall is approached, as expected, the shear-rate parameter increases and the Reynolds number decreases. In the
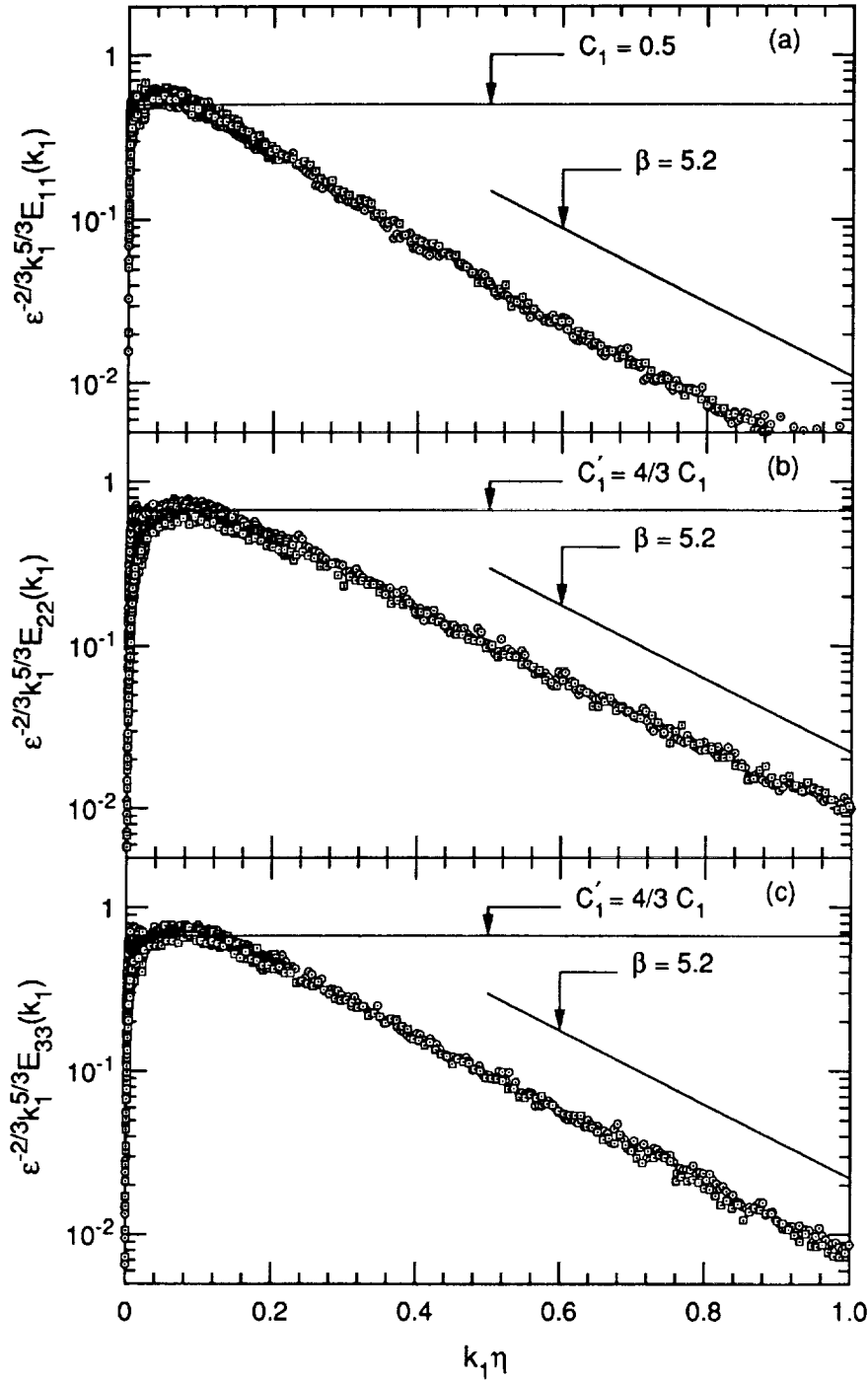
FIGURE 15. Log-linear plot of compensated spectra measured for $U_e \approx 10 \ m/s$ at different locations in the boundary layer. (a) u-spectrum; (b) v-spectrum; (c) w-spectrum. □ ; $y/\delta \approx 0.025$ and $R_\lambda \approx 400$ (log-layer), ○ ; $y/\delta \approx 0.5$ and $R_\lambda \approx 600$ (mid-layer).
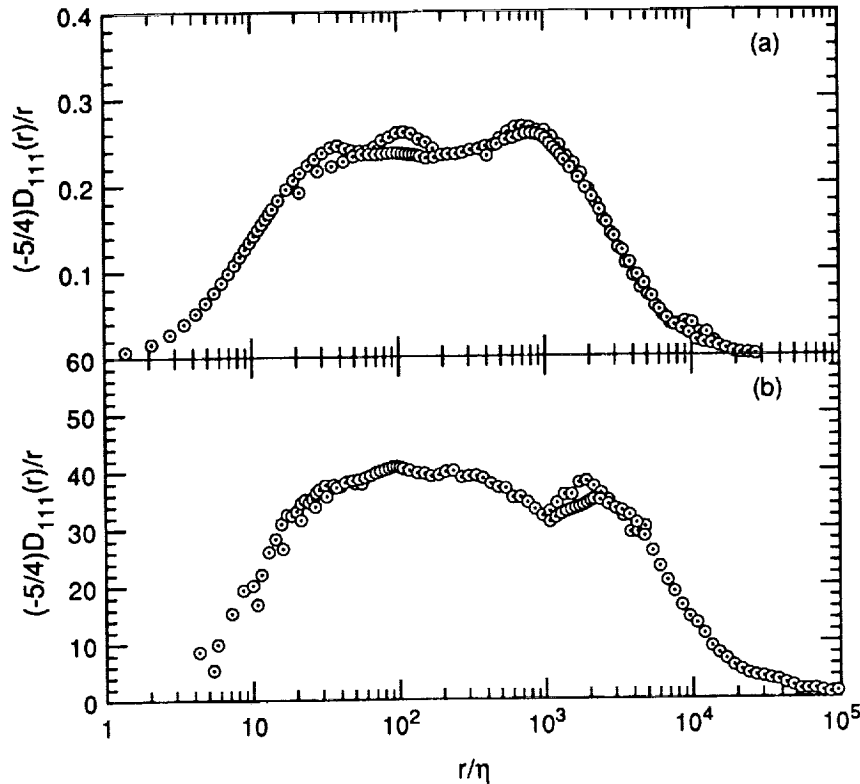
FIGURE 16. Compensated third-order structure functions for longitudinal velocity fluctuations measured around mid-layer. (a) $U_e \approx 10 \ m/s$, $R_\lambda \approx 600$; (b) $U_e \approx 50 \ m/s$, $R_\lambda \approx 1500$.

log-layer, comparison of the results taken at two freestream velocities gave some support to the conclusion of the above section that for the same y/δ the behavior of spectra for different freestream velocity was apparently determined only by the magnitude of the Reynolds number. The order in which the different components of spectra deviate from the −5/3 region, when the Reynolds number is decreased, is v, w, and then u. Referring back to Figure 15, which shows the exponential decay of the three components of spectra, it appears that the data for the near-wall position $(y/\delta \approx 0.025)$ agree with the mid-layer measurements in the dissipation region. This perhaps implies some universality of the dissipating scales.

3. Future plans

The immediate task is to analyze all of the data completely. Also, it is important that the concept of local isotropy is examined in a variety of high-Reynolds-number flows with different amount of mean strain. This should enable us to establish a relationship between the degree of anisotropy of the small scales and the magnitude of the mean strain, if such a relation should exist. One possible experiment is the case where an initially two dimensional turbulent boundary layer, which has been developed on a flat plate, is forced to encounter an obstacle placed vertically
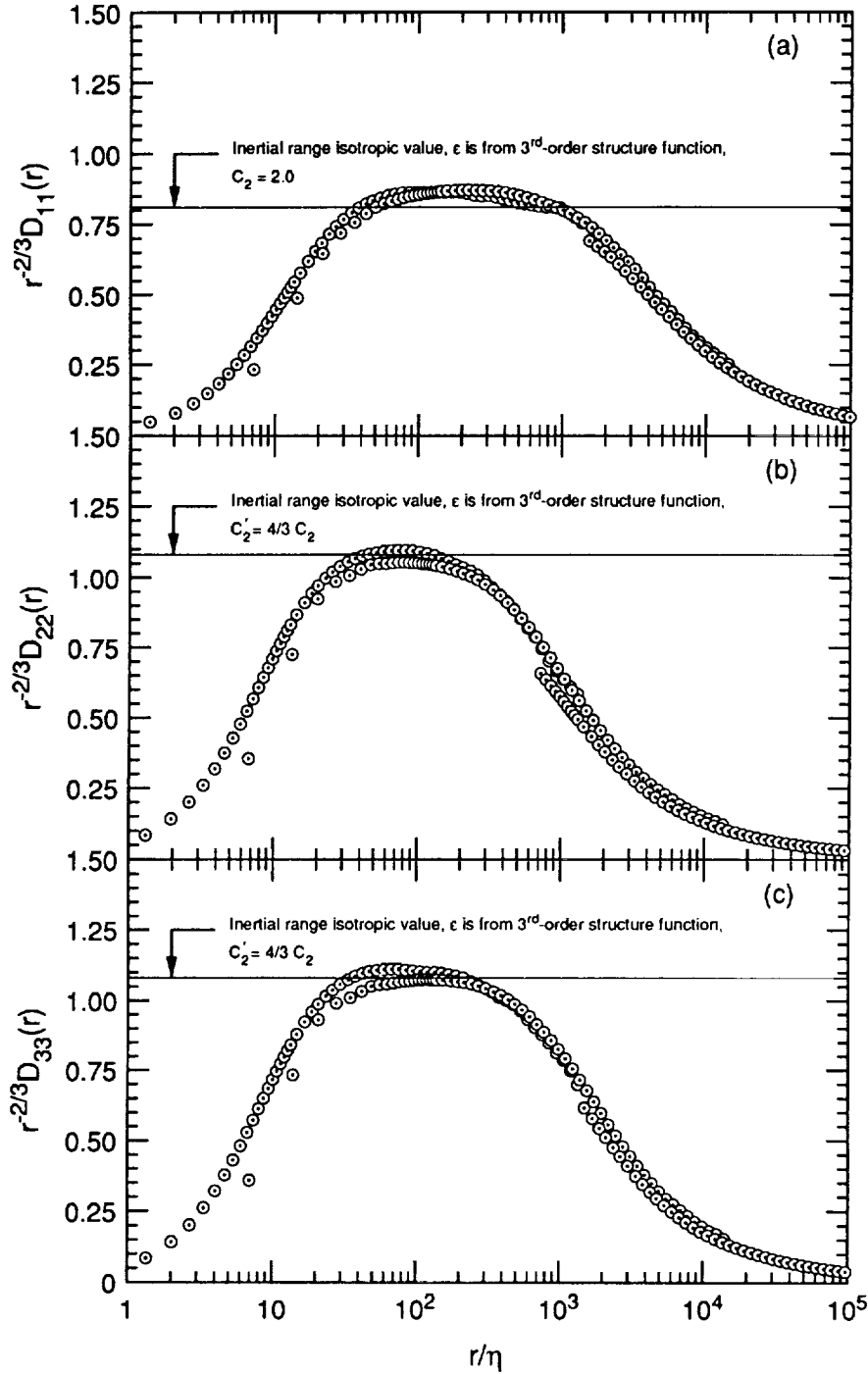
FIGURE 17. Compensated second-order structure functions for longitudinal and transverse velocity fluctuations measured around mid-layer for $U_e \approx 10$ m/s and $R_\lambda \approx 600$. (a) u; (b) v; (c) w.

in the boundary layer (e.g. a cylinder placed with its axis perpendicular to the plate). In this type of boundary layer, the pressure rises strongly as the obstacle is approached and in the imaginary plane of symmetry of the flow the boundary layer is also influenced by the effects of lateral straining. The size of this cylinder should be of the order of the thickness of the boundary layer. To conduct such an experiment in the 80' by 120' wind tunnel, a cylinder, which its diameter and length are approximately 1 m and 2 m respectively, are to be fixed to the ceiling of the tunnel. This presents an enormous amount of construction difficulties. However, we are investigating the possibilities of conducting such experiments.

REFERENCES

ANTONIA, R. A. & KIM, J. 1992 Isotropy of small-scale turbulence. *Proceedings of the Summer Program of the Center for Turbulence Research.* Stanford Univ./NASA Ames.

ANTONIA, R. A., KIM, J. & BROWNE, R. A. 1991 Some characteristics of small-scale turbulence in a turbulent duct flow. *J. Fluid Mech.* **233**, 369.

BATCHELOR, G. K. 1953 *The Theory of Homogeneous Turbulence. Cambridge University Press.*

CHAMPAGNE, F. H., FRIEHE, C. A., LA RUE, J. C. & WYNGAARD, J. C. 1977 Flux measurements, flux estimation techniques and fine scale turbulent measurements in the surface layer over land. *J. Atmos. Sci.* **34**, 515.

CHAPMAN, D. 1979 Computational aerodynamics development and outlook. *AIAA J.* **17**, 1293.

CORRSIN, S. 1958 On local isotropy in turbulent shear flow. *Report NACA R & M 58B11*.

DURBIN, P. A. & SPEZIALE, C. G. 1991 Local anisotropy in strained turbulence at high Reynolds numbers. *Recent Advances in Mechanics of Structured Continua.* **117**, 29.

EWING, D. W. & GEORGE, W. K. 1992 Spatial resolution of multi-wire probes. 45th *Annual Meeting of the Fluid Dynamics Division of the American Physical Society, Tallahassee.*

GEORGE, W. K. & HUSSEIN, H. J. 1991 Locally axisymmetric turbulence. *J. Fluid Mech.* **233**, 1.

KERR, R. M. 1990 Velocity, scalar and transfer of spectra in numerical turbulence. *J. Fluid Mech.* **211**, 309.

KIDA, S., KRAICHNAN, R. H., ROGALLO, R. S., WALEFFE, F. & ZHOU, Y. 1992 Triad interactions in the dissipation range. *Proceedings of the Summer Program of the Center for Turbulence Research.* Stanford Univ./NASA Ames.

KIDA, S. & MURAKAMI, Y. 1987 Kolmogorov similarity in freely decaying turbulence. *Phys. Fluids A.* **30**, 2030.

KOLMOGOROV, A. N. 1941 The local structure of turbulence in incompressible viscous fluid for very large Reynolds numbers. *C. R. Acad. Sci U.R.S.S.* **30**, 301.

KOLMOGOROV, A. N. 1962 A refinement of previous hypotheses concerning the local structure of turbulence in a viscous incompressible fluid at high Reynolds number. *J. Fluid Mech.* **13**, 82.

KRAICHNAN, R. H. 1959 The structure of isotropic turbulence at very high Reynolds numbers. *J. Fluid Mech.* **5**, 497.

LANDAU, L. D. & LIFSHITZ, E. M. 1987 *Fluid Mechanics. Pergamon Press.*

LEE, M. J., KIM, J. & MOIN, P. 1990 Structure of turbulence at high shear rate. *J. Fluid Mech.* **216**, 561.

LUMLEY, J. L. 1965 Interpretation of time spectra measured in high-intensity shear flows. *Phys. Fluids.* **8**, 1056.

MOIN, P. 1990 Similarity of organized structures in turbulent shear flows. *Near-Wall Turbulence, S. J. Kline and N. H. Afgan (eds.), New York, Hemisphere Publishers, 2.*

MESTAYER, P. 1982 Local isotropy and anisotropy in a high-Reynolds-number turbulent boundary layer. *J. Fluid Mech.* **125**, 475.

MESTAYER, P., CHOLLET, J. P., & LESIEUR, M. 1983 Inertial subrange of velocity and scalar variance spectra in high-Reynolds-number three-dimensional

turbulence. *Turbulence and Chaotic Phenomena in Fluids*, T. Tatsumi (ed.), Elsevier Science Publishers, 285.

NELKIN, M. & NAKANO, T. 1983 How do the small scales become isotropic in Navier-Stokes turbulence?. *Turbulence and Chaotic Phenomena in Fluids*, T. Tatsumi (ed.), Elsevier Science Publishers, 319.

PERRY, A. E. 1982 *Hot-Wire Anemometry*. Claredon Press Oxford.

SADDOUGHI, S. G. & VEERAVALLI, S. V. 1992 Local isotropy in high Reynolds number turbulent shear flows. *CTR Manuscript 140*. Center for Turbulence Research, Stanford Univ./NASA-Ames.

SAFFMAN, P. G. 1992 Vortical states, vortex filaments, and turbulence. *Review Tutorials, Summer Program of the Center for Turbulence Research*. Stanford Univ./NASA Ames.

SANADA, T. 1992 Comment on the dissipation-range spectrum in turbulent flows. *Phys. Fluids A*. 4, 1086.

SMITH, L. M. & REYNOLDS, W. C. 1991 The dissipation-range spectrum and the velocity-derivative skewness in turbulent flows. *Phys. Fluids A*. 3, 992.

SREENIVASAN, K. R. 1985 On the fine-scale intermittency of turbulence. *J. Fluid Mech.* 151, 81.

TAYLOR, G. I. 1935 Statistical theory of turbulence. *Proc. Roy. Soc. Lond. A*. 151, 421.

VEERAVALLI, S. V., & SADDOUGHI, S. G. 1991 A preliminary experimental investigation of local isotropy in high-Reynolds-number turbulence. *Annual Research Briefs of Center for Turbulence Research*. Stanford Univ./NASA Ames.

WILLIAMS, R. N. & PAULSON, C. A. 1978 Microscale temperature and velocity spectra in the atmospheric boundary layer. *J. Fluid Mech.* 83, 547.

WYNGAARD, J. C. 1968 Measurements of small-scale turbulence structure with hot wires. *J. Sci. Instrum.* 1, 1105.